Title: Metabolic retraction and virulence expansion in a tropical urban river microbiome under dry-season stress

Muhammad Ehteshamul Haque[1], Md. Shaminur Rahman[2], Munawar Sultana[1], Anowara Beguma[1]*

[1] Department of Microbiology, University of Dhaka, Dhaka-1000, Bangladesh

[2] Department of Microbiology, Jashore University of Science and Technology, Jashore-7408, Bangladesh

***Corresponding author**

Email: anowara@du.ac.bd (AB)

Corresponding Co-Author: munawar@du.ac.bd (MS)

Abstract

Anthropogenic pollution and seasonal flow reduction concentrate untreated organic waste in tropical rivers, yet the coupled response of microbial metabolism and virulence gene repertoires remains poorly understood. We applied shotgun metagenomics to the Shitalakshya River (Bangladesh) from early (December 2024) to peak (February 2025) dry season. Dissolved oxygen fell to near-hypoxic levels, ammonia nearly doubled (5.1 → 9.95 mg L^{-1}), and total organic carbon surged. KEGG profiling revealed a contracting metabolic core, with amino acid, carbohydrate, and energy metabolism declining by 59–86%, while xenobiotic biodegradation rose 4.6-fold and secondary metabolite biosynthesis 7.4-fold. Network analysis segregated the microbiome into a shrinking

growth-associated module and an expanding detoxification cluster. Parallel virulence gene profiling (VFDB) uncovered a 39% increase in total abundance and a 29% richer gene repertoire. Motility and chemotaxis genes nearly doubled, biofilm determinants (*algD, alg8, mrk* operon) emerged de novo, and Type VI secretion system components became markedly enriched. Conversely, siderophore-mediated iron acquisition and immune evasion factors declined substantially. These coordinated shifts indicate a transition from growth-oriented metabolism to persistence strategies based on environmental sensing and surface colonization. The co-enrichment of motility, biofilm, and T6SS traits alongside pollution-responsive pathways highlights a dual ecological filter wherein dry-season stress simultaneously selects for xenobiotic-tolerant generalists and opportunistic pathogens. Our findings establish a quantitative framework linking seasonal pollution to enhanced pathogenicity potential in urban rivers, with direct implications for drinking water abstraction and public health monitoring.

Keywords: metagenomics, virulence factors, KEGG (Kyoto Encyclopedia of Genes and Genomes) pathways, Type VI secretion system, xenobiotic degradation.

1. Introduction

Urban rivers in rapidly developing tropical regions are increasingly strained by untreated domestic and industrial wastewater, transforming them into conduits of concentrated organic and chemical pollutants [1–4]. This anthropogenic burden is severely compounded during the dry season, when diminished river flow reduces dilution capacity, leading to sharp declines in dissolved oxygen, accumulation of ammonia, and surges in total organic carbon [5–8]. This phenomenon is exacerbated by the resuspension of organic-rich sediment, which can dramatically increase biological oxygen demand and

create or worsen hypoxic conditions [9]. Such physicochemical deterioration pushes aquatic ecosystems toward hypoxic and eutrophic states that impose extreme energetic and redox stress on resident microbial communities [10,11]. While metagenomic surveys of polluted rivers have revealed extensive taxonomic shifts and enrichment of antibiotic resistance genes [12–14], the coupled reprogramming of core metabolic pathways and virulence-associated traits under intensifying dry-season stress remains poorly understood.

Microbial communities adapt to environmental adversity through coordinated functional transitions. In model systems, nutrient limitation and oxidative stress trigger stringent responses that downregulate translation, amino acid biosynthesis, and central carbon metabolism while upregulating stress-protective and detoxification modules [15–17]. In freshwater environments, eutrophication and hypoxia have been associated with shifts toward anaerobic energy metabolism and enhanced capacity for xenobiotic degradation [18–20]. However, whether these metabolic adjustments occur in concert with changes in virulence factor (VF) gene repertoires and what functional trade-offs govern such transitions have not been systematically addressed. This gap is particularly pressing because many fitness determinants annotated as virulence factors such as flagella, biofilm components, and Type VI secretion systems (T6SS), also confer selective advantages in extra-host environments, potentially enabling opportunistic pathogens to thrive under polluted conditions [21–25].

Emerging evidence indicates that environmental pollution can inadvertently enrich pathogen-associated traits. Wastewater-impacted rivers harbor elevated loads of motility, biofilm, and secretion system genes, often linked to genera that include serious

opportunistic pathogens [26–28]. Co-selection of stress tolerance and virulence may occur when the same regulatory networks govern responses to physicochemical challenges and expression of colonization factors [29].

Recent spatially resolved metagenomic studies along pollution gradients, such as those in the Kathajodi River, India, have demonstrated that catchment areas receiving untreated urban wastewater exhibit distinct enrichment of fecal-associated bacteria (*Bacteroides*, *Flavobacterium*, *Arcobacter*) and a broader repertoire of resistance and virulence genes compared to upstream sites [30,31]. These spatial patterns suggest that anthropogenic inputs function as strong ecological filters, reshaping community structure and functional potential.

Yet, the extent to which dry-season pollution simultaneously reshapes metabolic capabilities and virulence potential within a naturally assembled river microbiome has not been quantified through integrated metagenomic analysis. Understanding this dual reprogramming is essential to evaluate the public health implications of urban freshwater degradation, particularly in settings where river water is used for drinking, bathing, and irrigation [1,32]. Here, we applied shotgun metagenomics to the Shitalakshya River, a tropical urban river in Bangladesh that receives substantial untreated sewage and organic waste, to track the functional trajectory of the planktonic microbiome from the early to the peak of the dry season (December 2024 to February 2025). Concomitant sharp declines in dissolved oxygen, doubling of total organic carbon, and rising ammonia provided a natural experimental setting to test the hypothesis that extreme dry-season stress drives a coordinated metabolic retraction and virulence expansion in the microbial community. By integrating KEGG pathway profiling with comprehensive virulence factor gene

cataloging using VFDB [33], we aimed to (i) delineate the global metabolic reprogramming under pollution-induced stress, (ii) characterize shifts in virulence-associated gene abundance and diversity, and (iii) examine functional trade-offs between core anabolism and traits linked to environmental persistence and interbacterial competition. Our results reveal a system-scale ecological transition toward a stress-adapted, pathogen-enriched community state and introduce a compositional metric that may serve as a molecular index of ecological stress in polluted surface water.

2. Materials and methods

2.1 Study area

The study was conducted at the Sarulia intake point (23°43′02″ N, 90°30′00″ E) on the Shitalakshya River in Narayanganj, Bangladesh (Supplementary Fig. 1). This site is the primary raw water source for the Saidabad Water Treatment Plant (Phases I and II), the country's largest surface water treatment facility, which supplies drinking water to millions of residents in Dhaka.

2.2 Sample collection and rationale

Water sampling was conducted during two hydrologically distinct dry-season periods, early dry season (December 2024) and peak dry season (February 2025), to capture contrasting environmental conditions associated with progressive flow reduction and pollutant concentration in the river system. Rather than representing continuous seasonal monitoring, these two targeted time points were selected to reflect hydrological extremes within the dry season, when reduced river discharge and diminished dilution capacity intensify anthropogenic pollution stress and alter microbial community dynamics. The

environmental relevance of this sampling window is substantiated by operational evidence: during this period, deterioration of raw water quality at the intake of the Saidabad Water Treatment Plant necessitated the implementation of additional biological pre-treatment prior to conventional treatment processes [6].

At each time point, surface water samples (upper 0.5 m) were collected from the midstream region at the drinking water abstraction zone using sterile 2 L high-density polyethylene (HDPE) bottles. Triplicate water samples (n = 3 per site, 2 L each; 6 L total per site) were collected independently on the same day to account for local spatial and analytical variability within the sampling site. The midstream location was selected to minimize bank-associated heterogeneity and to better represent the mixed water column entering the treatment plant intake. Samples were immediately placed on ice, transported to the laboratory, and stored at 4 °C before processing to minimize biological alteration. Each 2 L replicate was partitioned as follows: 1 L for DNA extraction; 1 L for physicochemical and nutrient analyses (500 mL unfiltered for physicochemical and TOC measurements and 500 mL filtrate was used for nutrient determination and UV_{254} absorbance measurement). This allocation ensured sufficient volume for all downstream analyses while maintaining true field replication.

Although sediment can serve as a long-term reservoir and sink for pollutants, antibiotic resistance genes, and microbial contaminants in flowing river systems, the present study specifically focused on the water column because it directly represents the fraction abstracted for drinking water treatment and therefore poses the most immediate public health relevance.

By leveraging a targeted paired-sampling design, this approach generates a high-contrast view of dry-season stress, pinpointing key microbial metabolic and virulence shifts under acute pollution. The findings carry direct operational significance for safeguarding drinking water quality at the point of abstraction.

2.3 Physicochemical analysis

Physicochemical parameters pH, temperature, turbidity, conductivity, total dissolved solids (TDS), salinity, and dissolved oxygen (DO) were measured on a 500 mL unfiltered aliquot using calibrated multiparameter probes (HQ30d/HQ40d), a conductivity meter (MM150), and a portable turbidimeter (2100Q; all HACH, USA). Nutrient concentrations (NH_3–N, NO_2–N, NO_3–N) and UV_{254} absorbance were determined from the non-acidified filtrate (~500 mL) using a UV-VIS DR-6000 spectrophotometer (HACH, USA) following standard APHA methods [34]. Total organic carbon (TOC) was quantified from a 40 mL unfiltered aliquot using a Sievers InnovOx ES laboratory TOC analyzer with autosampler (Veolia, USA) based on supercritical water oxidation. All instruments were calibrated per the manufacturer's specifications.

2.4 DNA extraction

Microbial biomass from each 1 L replicate was collected on 0.22 µm membrane filters. Total DNA was extracted with the PowerWater DNA Isolation Kit (Qiagen). Integrity and purity were confirmed by agarose gel electrophoresis (0.8%) and A_{260}/A_{280} spectrophotometry (NanoDrop 2000, Thermo Scientific), respectively. DNA was stored at −20 °C until library preparation.

2.5 Library preparation and shotgun metagenomic sequencing

Metagenomic libraries were prepared using a modified Nextera XT–based (iNextEra) tagmentation protocol. Briefly, DNA (2.5 µL) was tagmented with bead-linked transposomes (Illumina DNA Library Prep) and 2× TMP buffer [35] in a 6 µL reaction at 53 °C for 30 min. Adapter ligation and dual indexing were performed by limited-cycle PCR using custom iNextEra primers with Q5 High-Fidelity DNA Polymerase (New England Biolabs). Cycling conditions were: strand repair at 72 °C for 3 min; initial denaturation at 98 °C for 3 min; 12 cycles of 98 °C for 45 s, 62 °C for 30 s, and 72 °C for 2 min; and final extension at 72 °C for 1 min. Amplified libraries (300–700 bp) were verified by agarose gel electrophoresis, quantified using a Qubit Flex fluorometer (Thermo Fisher Scientific), normalized, pooled, and purified with AMPure XP beads (Beckman Coulter). Paired-end sequencing (2 × 150 bp) was performed on an Illumina NovaSeq X Plus platform (Novogene). The raw metagenomic sequence data have been submitted to the NCBI's Sequence Read Archive (SRA) under the BioProject ID PRJNA1424261 (https://www.ncbi.nlm.nih.gov/bioproject/PRJNA1424261) (Accession: SAMN55380971 and SAMN55380975).

2.6 Taxonomic classification and functional annotation of metagenomic sequences

Initial quality evaluation of raw FASTQ files was conducted using FastQC [36]. Adapter trimming and quality filtering were carried out with Trimmomatic [37] employing strict parameters: a 4 bp sliding window, a minimum Phred quality score of 20, and a minimum

read length of 50 bp. On average, 70.51 million read pairs per sample were retained post-filtering (range: 52.98–81.91 million pairs). To enrich for microbial sequences, host-derived reads were filtered out using BBduk from the BBtools package [38]. This step was performed *in silico* by aligning the quality-trimmed reads against the human reference genome (GRCh38, GCA_000001405.15_GRCh38_no_alt_analysis_set.fna) using a k-mer length of 31. Reads that did not align to the host genome were retained as "host-filtered" and used for downstream taxonomic profiling. Filtered reads were classified taxonomically using Kraken2 [39] with a confidence threshold of 0.1 and a minimum of 2 hit groups required for classification. The analysis was performed against a custom Kraken2 database, a prebuilt Kraken2 database, last updated in July 2025 (https://benlangmead.github.io/aws-indexes/k2). The database included archaeal, bacterial, viral, and fungal genomes from RefSeq or other standard sources, though the exact composition is user-defined. The Kraken2 classification reports were subsequently processed with Bracken [40] to achieve more accurate species-level abundance estimates. Taxonomic identification was enhanced using TaxonKit [41]. Detailed sequencing quality-control metrics, including trimming efficiency, host-read removal, and microbial-read classification statistics, are provided in S1 Dataset.

Functional profiling of antimicrobial resistance was performed using the AMR++ pipeline [42]. High-quality reads were mapped to the MEGARes database (v2.0) [42,43]. Only gene matches with ≥99% sequence coverage were retained to ensure specificity. The resulting high-confidence gene identifications were analyzed using ResistomeAnalyzer (v2.1; https://github.com/cdeanj/resistomeanalyzer) to characterize antimicrobial resistance profiles. This stringent filtering minimized partial matches and enhanced the

accuracy of resistome profiling. Reads Per Kilobase (RPK) gene family abundance tables from HUMAnN3 [44] were processed to consolidate UniRef90 IDs and remove taxonomic annotations. Gene abundances were summed for each UniRef90 identifier to eliminate redundancy. This pipeline ensured comprehensive metabolic profiling while maintaining compatibility with downstream statistical and comparative analyses.

2.7 Data analysis

All statistical analyses were performed in R (v4.2.0) using RStudio (2022.07.1). Comparative analyses of water quality parameters and functional gene abundances between sampling periods were conducted using appropriate parametric or non-parametric tests following assessment of data normality and homogeneity of variance [45–48]. Figures were generated using reproducible scripts within the R statistical environment.

3. Results

3.1 Water quality deterioration

Physicochemical parameters captured a clear decline in water quality from the early dry season (December 2024) to the peak dry season (February 2025) (**S1 Table)**. Dissolved oxygen dropped sharply from 1.55 to 0.54 mg/L, indicating severely hypoxic conditions, while ammoniacal nitrogen increased more than threefold from 3.01 to 10.03 mg/L. Total organic carbon (TOC) showed a dramatic 5.47-fold increase (3.2 to 17.5 mg/L), and turbidity rose from 15.8 to 37.27 NTU (2.36-fold). These changes were accompanied by increases in conductivity (452.94 to 748.36 µS/cm), UV_{254} absorbance (0.09 to 0.20

cm^{-1}), and color (15.63 to 52.2 Pt-Co), collectively indicating elevated organic, particulate, and nutrient loading during the peak dry season.

3.2 Global metabolic reprogramming revealed by KEGG pathways

At the highest functional level, the metagenome underwent a sweeping redistribution (**Fig 1**). Metabolism remained the largest category but contracted from 70.3% to 62.5% of annotated reads. This decline was offset by substantial expansions in Human Diseases (from 8.0% to 13.4%), Organismal Systems (1.5% to 7.6%), and Cellular Processes (0.5% to 4.8%), while Genetic Information Processing halved from 16.6% to 8.0% and Environmental Information Processing decreased modestly from 2.5% to 3.7%. Such a sweeping redistribution of functional potential signals a systemic shift from growth-oriented metabolism toward stress adaptation and defense.

Fig 1. Global KEGG pathway class distribution in December 2024 and February 2025. Pie charts showing the relative abundance (%) of six major functional categories. Metabolism contracts while Human Diseases, Organismal Systems, and Cellular Processes expand.

3.3 Pollution-Induced Shifts in Microbial Functional Potential

To assess the impact of pollution stress on microbial community function, we analyzed the relative abundance of metabolic pathways and functional subclasses between December 2024 and February 2025. The data reveals a significant shift in functional

profiles, characterized by an upregulation of stress-response and detoxification pathways and a marked downregulation of core growth and biosynthesis pathways.

3.3.1 Shifts in Functional Subclasses

The analysis of key functional subclasses (**Fig 2**) highlights a distinct divergence between defense mechanisms and central metabolism. Pathways associated with stress tolerance and environmental interaction showed robust increases in relative abundance. Most notably, *Xenobiotics biodegradation and metabolism* exhibited the largest positive change, increasing by +8.1% (from ~2.5% to ~10.5%). Other pathways that significantly increased include *Biosynthesis of other secondary metabolites* (+5.5%), *Lipid metabolism* (+3.6%), *Metabolism of terpenoids and polyketides* (+2.7%), and *Infectious disease: bacterial* (+2.6%). Conversely, pathways fundamental to microbial growth and energy production experienced substantial reductions. *Amino acid metabolism* showed the steepest decline, dropping by -10.0% (from ~17.5% to ~7.5%). Significant decreases were also observed in *Energy metabolism* (-6.9%), *Nucleotide metabolism* (-6.6%), *Translation* (-6.1%), and *Carbohydrate metabolism* (-4.5%). These opposing trends indicate a functional restructuring away from anabolic growth processes toward survival, adaptation, and detoxification.

Fig 2. Functional restructuring under pollution stress. This dumbbell plot shows the shift in microbial pathway abundance from December 2024 to February 2025. Core growth and biosynthetic pathways (e.g., Amino acid and Energy metabolism) decreased significantly (red lines), while stress-response and detoxification pathways (e.g.,

Xenobiotics biodegradation) increased (green lines), reflecting a community-wide shift from growth to survival.

3.3.2 Biological Importance and Magnitude of Change

To further contextualize these shifts, we plotted the February 2025 abundance against the December 2024 abundance, with point size indicating biological importance (Abundance × Change Magnitude) and shape denoting pathway type (**Fig 3**). Consistent with the subclass analysis, Xenobiotics biodegradation and metabolism emerge as a critical node, showing a high fold change (FC: 4.63x) and positioning significantly above the dashed line of no change. Lipid metabolism also shows a strong positive shift (FC: 1.92x). In contrast, pathways such as Amino acid metabolism (FC: 0.41x) and Carbohydrate metabolism (FC: 0.63x) fall below the baseline, confirming a reduction in abundance.

Fig 3. Pathway Importance and Change Analysis. This scatter plot visualizes the shift in microbial pathway abundance before (December 2024, x-axis) and after (February 2025, y-axis) pollution stress. The dashed diagonal line represents no change; points above the line increased in abundance, while points below decreased. Marker size indicates biological importance (abundance × fold change), and color/shape denotes functional class. Key anabolic pathways (e.g., Amino acid and Energy metabolism) shifted below the line, indicating decline, whereas detoxification and stress pathways (e.g., Xenobiotics biodegradation and Infectious disease) surged above the line with high fold changes.

Despite its low absolute abundance, Infectious disease: bacterial exhibits a dramatic fold change (FC: 22.33x), and Signaling molecules and interaction shows an infinite fold change (emerging from near-zero levels), suggesting that even low-abundance stress-response pathways are being heavily activated. Energy and translation-related pathways remained clustered in the lower abundance range with fold changes near 0.3x, reinforcing the conclusion that pollution stress suppresses microbial growth machinery in favor of survival mechanisms.

3.4 Integrated KEGG network analysis reveals ecological resilience of the river microbiome

KEGG pathway interaction network analysis demonstrated pronounced functional reorganization of the Shitalakshya River microbiome during the dry-season period (December 2024–February 2025). Central network modules (**Fig 4**) were dominated by metabolism-associated pathways, including carbohydrate, amino acid, lipid, and nucleotide metabolism, which exhibited high connectivity and interaction density, indicating coordinated metabolic adaptation under environmentally stressed conditions. Pathways related to genetic information processing, particularly translation and replication/repair, were tightly integrated with core metabolic functions, suggesting sustained microbial growth and active cellular maintenance. In contrast, several peripheral functional clusters displayed directional shifts in abundance, reflecting selective enrichment or suppression of specific ecological processes. Notably, xenobiotic biodegradation pathways remained strongly connected within the network, consistent with adaptive responses to anthropogenic contamination pressure. Collectively, the

network topology indicates that metabolic and information-processing pathways underpin the ecological resilience and functional stability of the riverine microbiome during seasonal environmental perturbation.

Fig 4. KEGG Pathway Interaction Network. Network diagram showing functional shifts in the Shitalakshya River microbiome (Dec 2024 – Feb 2025). Nodes represent pathways; node size reflects average abundance, fill color shows functional class, and border color indicates change direction (blue = decreased, red = increased). The network reveals a stark division: core biosynthetic and metabolic pathways (left cluster) declined, while stress-related and disease pathways (right clusters) increased in abundance.

3.5 Dry-season stress enriches a functionally coherent consortium of xenobiotic-degrading and disease-associated microorganisms

The 4.6-fold enrichment in community-level xenobiotic biodegradation capacity (from 2.22% to 10.27% of annotated KEGG reads) between December 2024 and February 2025 was accompanied by a profound restructuring of the Shitalakshya River microbiome, characterised by the selective proliferation of two ecologically intertwined but clinically distinct bacterial guilds: canonical xenobiotic degraders and opportunistic human pathogens.

3.5.1 Specialized xenobiotic-degrading consortium emerges.

The functional surge in pollutant catabolism was underpinned by the disproportionate expansion of a phylogenetically diverse but metabolically coherent assemblage of degraders. The most extreme enrichment was observed for *Achromobacter aegrifaciens*, an emerging degrader of organopollutants, which surged 1,945-fold from near-detection limits (20 reads) to dominance (38,896 reads; Log_2 fold change = +10.93; adjusted $P < 0.001$; **Fig 5a**). This was accompanied by parallel expansions of *Brevundimonas diminuta* (28.6-fold; 86,600 → 2,481,257 reads), a hydrocarbon degrader, and *Comamonas testosteroni* (9.5-fold; 110,297 → 1,043,615 reads), renowned for steroid and plastic catabolism (**S2 Table)**. Unclassified *Pseudomonas* species expanded 8.3-fold (42,527 → 352,601 reads), suggesting a substantial reservoir of uncharacterized catabolic potential. Critically, this enrichment was sharply (Roges et al., 2020; Wang et al., 2023selective: *Thauera humireducens*, an aromatic degrader, collapsed 25-fold (19,869 → 849 reads), while *Acidovorax temperans* declined 0.6-fold (117,948 → 72,764 reads), indicating that the dry-season physicochemical regime characterized by elevated pollutant concentrations, hypoxia, and reduced flow imposed a stringent ecological filter favoring a specific subset of the degrading guild (**Fig 5b**). This filter favored a specific cohort of organisms, predominantly within the *Pseudomonadota*, exhibiting a combination of versatile catabolism, hypoxia-tolerance, and robust stress-response systems. The co-enrichment of *Pseudomonas putida* and a vast pool of uncharacterized *Pseudomonas* species (8.3-fold increase to 35% of the genus-level reads) further indicates that much of this environment's xenobiotic degradation potential resides in a flexible and rapidly responding functional guild, not a single taxonomic group.

Fig 5. Selective enrichment of a xenobiotic-degrading consortium under dry-season conditions. (a): Volcano plot of differential bacterial abundance between December 2024 and February 2025. Each point represents a species. Significantly enriched (red; Log_2 fold change > 1, adjusted $P < 0.05$) and depleted (blue; Log_2 fold change < −1, adjusted $P < 0.05$) taxa are highlighted against non-significant background species (grey). Dashed lines denote statistical thresholds. The most extreme responders, *Achromobacter aegrifaciens* (1,945-fold enriched) and *Thauera humireducens* (25-fold depleted) are labelled. (b) Dot plot heatmap showing the relative abundance (dot size) and enrichment fold change (dot colour) of 16 key xenobiotic-degrading species, grouped by substrate class (right sidebar). The heatmap highlights the selective nature of the enrichment across different catabolic guilds.

3.5.2 Concurrent enrichment of clinically relevant pathogens

Strikingly, this niche filter also selected for a broad array of disease-associated microorganisms, revealing a convergent ecological response where traits conferring fitness under environmental stress, such as multidrug efflux, biofilm formation, and broad substrate utilization, simultaneously potentiate opportunistic pathogenicity. Reads assigned to the major opportunistic pathogen *Pseudomonas aeruginosa* increased 7.1-fold (8,236 → 58,220), while the multidrug-resistant nosocomial pathogen *Stenotrophomonas maltophilia* rose 9.5-fold (2,554 → 24,346). The recently described bloodstream infection-associated *Stenotrophomonas pigmentata* exhibited a 325-fold expansion (107 → 34,775 reads). Several clinically significant species emerged *de novo* in the February 2025 metagenome, having been undetectable in

December 2024: *Clostridioides difficile* (0 → 277 reads), *Enterococcus faecalis* (0 → 137 reads), *Listeria monocytogenes* (0 → 244 reads), and *Pasteurella multocida* (0 → 236 reads) (**Fig 6; S3 Table)**. The most dramatic proliferation was observed for *Tissierella carlieri*, an emerging anaerobic opportunistic pathogen associated with soft tissue infections and bacteremia, which appeared *de novo* and reached 1,995,804 reads, becoming one of the most abundant single taxa in the February community. Similarly, *Aeromonas media*, an enteric pathogen causing diarrheal disease, surged 116.8-fold (12,596 → 1,470,792 reads), while *Clostridium tetani*, the causative agent of tetanus, expanded 171.5-fold (67 → 11,490 reads). The anaerobic opportunist *Bacteroides thetaiotaomicron* increased 248-fold (65 → 16,126 reads), and *Empedobacter falsenii*, a hospital-acquired bloodstream pathogen, rose 50.3-fold (14,723 → 739,932 reads). These expansions occurred alongside the persistence of high-risk pathogens at clinically concerning abundances: *Klebsiella pneumoniae* maintained a persistent high load (~48,000 reads at both time points), while *Morganella morganii* expanded 4.2-fold to 871,649 reads.

Fig 6. Lollipop chart of differentially abundant disease-associated species. Point colour indicates enrichment status; diamond shapes denote *de novo* emergence (absent in December 2024)

3.5.3 Ecological coupling of degradation and pathogenicity traits.

The co-enrichment of xenobiotic degraders and opportunistic pathogens was not taxonomically independent. Several of the most highly enriched taxa occupy both functional categories simultaneously. *Achromobacter xylosoxidans*, a known degrader of

aromatic compounds and herbicides (36.9-fold enrichment; 625 → 23,038 reads), is also a recognised opportunistic pathogen causing bacteremia and pneumonia in cystic fibrosis patients. *Brevundimonas diminuta*, which expanded 28.6-fold to dominate the community, couples hydrocarbon degradation with the capacity to cause catheter-related bacteremia and peritonitis. Pseudomonas aeruginosa, enriched 7.1-fold, is both a model xenobiotic degrader and a paradigmatic multidrug-resistant nosocomial pathogen. This dual functionality suggests that the genomic determinants of environmental stress tolerance, including broad-specificity efflux pumps, mobile genetic elements, and catabolic plasmids, may simultaneously encode or facilitate the acquisition of virulence-associated traits, blurring the boundary between environmental generalist and opportunistic pathogenicity.

3.5.4 Selective depletion of waterborne and zoonotic pathogens

In marked contrast to the enrichment of nosocomial and wound-associated opportunists, several classical waterborne pathogens declined precipitously. *Vibrio cholerae*, the causative agent of cholera, decreased from 9,970 to 632 reads, while *Vibrio parahaemolyticus* and *Vibrio fluvialis* fell to 656 and 95 reads, respectively. The foodborne pathogen *Yersinia enterocolitica* declined from 584 to 76 reads. These parallel declines suggest that the intensified dry-season conditions, particularly elevated salinity and reduced dissolved oxygen may have exceeded the physiological tolerance ranges of these typically estuarine and freshwater pathogens, even as they selected for the hypoxia-tolerant, biofilm-forming opportunists that dominated the enriched fraction.

3.5.5 Synthesis

Together, these taxonomic shifts reveal a deterministic ecological response to intensifying dry-season stress: the selective enrichment of a dual-functional microbial assemblage capable of both xenobiotic catabolism and opportunistic infection. The convergence of these traits in a single, co-enriched consortium dominated by *Achromobacter*, *Pseudomonas*, *Brevundimonas*, *Comamonas*, *Stenotrophomonas*, and anaerobic *Clostridium*/*Tissierella* lineages indicates that chronic pollution and hydrological stress may inadvertently cultivate a latent public health reservoir within urban riverine ecosystems. This coupling of biodegradative capacity and pathogenic potential represents an underexplored dimension of water quality deterioration in anthropogenically impacted tropical rivers.

3.6 Virulence factor dynamics

The comparative analysis of virulence factor (VF) profiles between December 2024 and February 2025 revealed a pronounced restructuring of functional traits under dry-season stress (**Fig 7**). While the overall composition remained structurally consistent across ten functional categories, substantial shifts in relative abundance indicate strong ecological reprogramming.

Fig 7. Stacked bar chart showing the relative abundance of major virulence factor categories in December 2024 and February 2025. A pronounced increase in motility-related factors is observed in February, accompanied by enrichment of biofilm formation, indicating enhanced dispersal and persistence under dry-season stress. In contrast,

nutritional/metabolic, immune modulation, and invasion-related functions declined, reflecting reduced investment in host-associated and energy-intensive processes.

3.7 Expansion and restructuring of virulence potential

Temporal metagenomic analysis revealed a significant expansion of virulence-associated genetic potential from early (December 2024) to peak dry season (February 2025). Total virulence factor (VF) abundance increased by 38.9% (from 46.02 to 63.91), accompanied by a 28.6% expansion in the number of detected VF genes (from 294 to 378; **Table 1**). This coordinated increase suggests a net gain in community-wide virulence capacity rather than a simple redistribution of existing genes.

Table 1. Temporal dynamics of virulence factor abundance and gene counts (December 2024 – February 2025).

Category	Abundance (Dec)	Abundance (Feb)	Δ Abundance	Genes (Dec)	Genes (Feb)	Δ Genes	Trend
Motility	19.35	33.58	+14.23	55	108	+53	↑↑
Biofilm formation	2.41	4.63	+2.22	8	13	+5	↑

Category	Abundance (Dec)	Abundance (Feb)	Δ Abundance	Genes (Dec)	Genes (Feb)	Δ Genes	Trend
Effector delivery system	22.68	22.88	+0.20	68	98	+30	↑
Adherence	22.89	21.37	-1.52	81	76	-5	↓
Nutritional/Metabolic factor	13.78	8.06	-5.72	51	55	+4	↓↓
Immune modulation	6.79	3.38	-3.41	18	16	-2	↓
Antimicrobial activity/Competitive advantage	6.47	4.07	-2.40	2	2	0	↓
Invasion	3.01	1.08	-1.93	4	6	+2	↓

Category	Abundance (Dec)	Abundance (Feb)	Δ Abundance	Genes (Dec)	Genes (Feb)	Δ Genes	Trend
Regulation	2.56	0.94	-1.62	4	3	-1	↓
Exotoxin	0.09	0.03	-0.06	3	1	-2	↓
TOTAL	46.02	63.91	+17.89	294	378	+84	↑

3.8 Motility and biofilm expansion

The most dramatic restructuring occurred within motility-associated genes, which surged from 19.35 to 33.58 in cumulative abundance (+14.23), making it the top category in February (**Fig 8**). Gene count in this class nearly doubled from 55 to 108, reflecting massive mobilization of flagellar and chemotaxis systems (**S1 Dataset)**. Specific flagellar motor and switch components *fliM* (0.65 → 1.92), *flgG* (0.49 → 1.16), *fliG*, and *flgI* showed substantial increases, while chemotaxis genes *cheW*, *cheB*, *cheY*, and *pomA2* became more abundant or appeared *de novo*.

Fig 8. Virulence factor abundance across functional categories during dry-season progression. Relative abundance of VF categories in December 2024 and February 2025. A pronounced increase in motility (Δ = +14.00) and biofilm formation (Δ = +2.00) was observed in February, indicating enhanced microbial dispersal and surface colonization

potential. In contrast, nutritional/metabolic functions (Δ = −7.00), immune modulation (Δ = −3.00), and antimicrobial activity (Δ = −2.00) declined.

Concomitantly, biofilm pathway genes displayed a marked upswing (+2.22 absolute). The alginate biosynthesis cluster (*algD*, *alg8*, *algE*, *algQ*, *algR*) was absent in December but reached notable levels in February, while type 3 fimbrial genes (*mrkA-F*) increased steadily, indicating enhanced potential for surface attachment and matrix production. The co-enrichment of motility and biofilm traits indicates a dynamic ecological balance between dispersal and surface-associated survival, potentially reflecting biofilm formation–dispersal cycles rather than mutually exclusive behaviors

3.9 Effector delivery systems remain robust with nuanced changes

Effector delivery systems, predominantly Type II, Type III, and Type VI secretion systems, remained the second most abundant class (**S1 Dataset)**, with a modest overall increase (22.68 → 22.88). The Type VI secretion system (T6SS) expanded robustly. The T6SS ATPase *clpB* emerged *de novo* (0 → 1.10), together with multiple *ats* genes (*atsC*, *atsH*, *atsJ*), contractile sheath subunits *vipA/tssB* and *vipB/tssC*, and the effector *vgrG2* (0 → 0.55). In contrast, some Type III secretion system effectors (*espL1*, *espX1*) declined, indicating a strategic shift toward T6SS-mediated interbacterial competition rather than eukaryotic cell manipulation.

3.10 Attenuation of iron acquisition systems and immune evasion mechanisms

Categories linked to nutrient acquisition and immune subversion decreased substantially **(S1 Dataset)**. Nutritional/metabolic factors decreased by 5.72 units (13.78 → 8.06), driven largely by reductions in siderophore biosynthesis and transport genes. The enterobactin system (*entA-F*, *fepA-G*) and aerobactin receptor *iutA* all exhibited marked attenuation, as did yersiniabactin-associated genes (*irp2*, *ybtS*, *ybtU*), many of which fell below detection. Immune modulation capacity declined by 3.41 units (6.79 → 3.38). Capsule assembly proteins (e.g., *KP1_RS17345*, *Wzi*) and lipopolysaccharide modification enzymes (*lpxC*, *waaC*, *waaG*) were strongly reduced or lost. Similarly, invasion-associated genes (*ibeB*, *ompA* variants) and exotoxins contracted. The attenuation of these traits likely reflects relaxed selection for host-associated functions and reduced iron limitation in hypoxic, organic-rich waters.

4. Discussion

The parallel application of KEGG pathway profiling and virulence factor (VF) gene cataloging to the Shitalakshya River, a tropical system under acute organic pollution, reveals a coherent, multidimensional microbiome stress response as dry-season conditions intensify. Over only two months, the metagenome shifted decisively away from biosynthesis and growth toward detoxification, motility, biofilm formation, and interbacterial competition, a transformation that simultaneously curtails core anabolism and enriches traits with direct implications for public health. This temporal functional trajectory is consistent with spatial patterns observed along pollution gradients in other

urban rivers, where catchment areas receiving untreated wastewater serve as hotspots for enrichment of resistance and virulence genes [12,49,50,20,47,30,31].

4.1 Ecological filtering of core metabolism

The collapse of central metabolism is the most conspicuous signature of environmental deterioration. Amino acid, carbohydrate, and energy metabolism, together with translation and nucleotide biosynthesis, contracted by 60–85%, forming a tightly connected module of suppressed functions. This coordinated downregulation mirrors the stringent response and stationary phase physiology known from model organisms, in which resource scarcity and redox stress halt ribosome production and anabolic pathways [51,52,17,24]. The sharp decline in dissolved oxygen to near-hypoxic levels, the doubling of total organic carbon, and the accumulation of toxic ammonia impose simultaneous energy limitation, carbon catabolite repression, and nitrogen stress [7,8,4]. The link between elevated organic matter in resuspended sediment and subsequent oxygen depletion, as modeled by Morote-Sánchez et al. [9], provides a mechanistic explanation for the severe hypoxia observed in the late dry season. Under such combined pressures, shutting down expensive anabolic machinery is a conserved survival strategy, as evidenced across aquatic metagenomes under eutrophic and hypoxic conditions [53,11,54,30]. The halving of genetic information processing capacity further indicates that the late dry-season community has entered a regime of profoundly reduced growth, likely reflecting a systemic metabolic shutdown in planktonic autochthonous bacteria.

4.2 Recruitment of detoxification modules

In place of core metabolism, we observed a massive induction of xenobiotic biodegradation and secondary metabolite biosynthesis. These pathways expanded as a distinct, loosely connected network module, decoupled from central carbon metabolism. This architecture suggests the recruitment of peripheral, often plasmid- or island-encoded catabolic pathways that operate with minimal interference with core processes. The 4.6-fold surge in xenobiotic degradation capacity, the enrichment of secondary metabolite biosynthesis, and the expansion of lipid metabolism point to the activation of detoxification and membrane remodeling mechanisms characteristic of pollutant-degrading specialists and biofilm-associated communities [18,19,50]. The concomitant rise in terpenoid/polyketide pathways further indicates extensive production of stress-protective compounds [29]. Thus, the community transitions from a growth-oriented metabolic economy to one centered on detoxification and chemical defense, a functional shift analogous to the enrichment of carbohydrate and xenobiotic metabolism in wastewater-impacted river sections [30].

4.3 Expansion and restructuring of virulence potential

A particularly consequential dimension of this reprogramming is the expansion and restructuring of virulence-associated genetic potential. Total virulence factor abundance increased by 39%, accompanied by a 29% increase in detected genes, indicating a net gain in community-wide pathogenic capacity [53,20,24,47,48,27].

Flagellar and chemotaxis gene counts nearly doubled, indicating enhanced capacity for directional movement toward nutrients and away from toxins, a process tightly regulated by the flagellar assembly machinery [65]. The *de novo* appearance of the full alginate

biosynthesis cluster, together with enhanced fimbrial genes, signals a heightened potential for surface colonization and matrix production [55,33,31].

Motility and biofilm are often viewed as opposing lifestyles. Still, their co-enrichment here supports the concept of biofilm formation dispersal cycles, where motile cells seed new surfaces and biofilm cells later release propagules, a dynamic bet-hedging strategy that maximizes persistence under fluctuating stress [56]. Elevated turbidity and TOC increase suspended organic particles that act as nutrient-rich microsites and attachment surfaces, promoting biofilm formation [57–59].

The robust expansion of the Type VI secretion system (T6SS) repertoire, including the emergence of key structural components (*clpB*, *vgrG2*) alongside an increase in pivotal sheath proteins, indicates a strategic pivot toward interbacterial competition [60,61]. T6SS functions as a contact-dependent weapon that injects toxic effectors into neighboring competitors; its upregulation is frequently associated with high cell density, surface-associated growth, and interspecies warfare. The parallel decline of Type III secreted effectors suggests a departure from eukaryotic cell-targeted virulence [62], consistent with the reduced immunological pressure in an environmental setting. In the resource-limited, high-density communities of the late dry season, T6SS-mediated killing can confer a strong fitness advantage, potentially favoring pathogens that double as effective microbial competitors.

4.4 Attenuation of iron acquisition and immune evasion

Remarkably, this heightened competitive and dispersal potential was accompanied by a strong attenuation of iron acquisition systems and immune evasion factors. Siderophore biosynthesis (enterobactin, aerobactin, yersiniabactin) and capsule/LPS modification

genes receded sharply [23,29]. In hypoxic, organic-rich sediments, iron bioavailability typically increases due to reductive dissolution and complexation with humic substances, thereby diminishing the selective advantage of high-affinity iron chelators. Simultaneously, the loss of immune-modulatory and invasion traits may reflect relaxed selection for host-associated functions in an extra-host environment, or a trade-off with the energy demands of stress survival [63]. The net effect is a community that combines enhanced environmental persistence and interbacterial competitiveness with a preserved, albeit altered, arsenal of virulence determinants [12].

4.5 Ecological and public health implications

The elevation of KEGG "Infectious disease: bacterial" pathways (a 23-fold increase) and the 38.9% rise in total VF content should not be interpreted as a simple increase in obligate pathogen load. Many VFDB-annotated genes—flagella, T6SS, and biofilm polysaccharides—are also fundamental ecological fitness factors. However, their amplification in a water body that serves as a source of drinking, bathing, and irrigation water raises legitimate concerns about the dissemination of opportunistic pathogens such as *Pseudomonas aeruginosa*, *Aeromonas* spp., and *E. coli*, which exploit these very traits for environmental survival and human infection [1,23]. The *de novo* appearance of quorum-sensing and signaling pathways hints at the activation of cell–cell communication networks that could synchronize virulence factor expression at the community scale, further amplifying risk [26]. These findings align with evidence that severe organic enrichment and hypoxia enhance the persistence of enteric pathogens [32,28].

4.6 A proposed ecological index of stress

By integrating KEGG functional profiling with VF enumeration, we propose a composite "xenobiotic degradation to translation ratio" (XD/T) as a potential molecular index of ecosystem stress. In December, XD/T was ~0.27 (2.22/8.23); by February, it jumped to 4.80 (10.27/2.14), an 18-fold increase. This ratio captures the fundamental trade-off between anabolic capacity (translation) and detoxification potential (xenobiotic degradation). Similar composite indices have been proposed in soil ecology (e.g., carbon quality indexes), and the XD/T ratio could be developed as a sensitive biomonitoring metric for assessing functional deterioration in polluted surface water systems. Metatranscriptomic validation will be required to confirm the active transcription of these pathways and to link them directly to pollutant concentrations.

4.7 Conceptual framework

Conceptual framework (Fig 9) illustrating the integrated dual-filter model of dry-season stress on the river microbiome. Seven hierarchical levels depict the cascade from environmental drivers to public health outcomes: (1) Environmental drivers (low flow, declining DO, rising NH_3 and TOC); (2) Metabolic retraction (suppression of amino acid, energy, and translation pathways); (3) Microbial community restructuring (enrichment of xenobiotic degraders and opportunistic pathogens); (4) Virulence factor dynamics (expansion of motility, biofilm, T6SS; contraction of iron acquisition and immune modulation); (5) Ecological mechanisms (energy trade-off, co-selection, regulatory cross-talk, environmental cues); (6) Ecosystem and public health outcomes; and (7) The XD/T ratio as a composite stress index (0.27 → 4.80, 18-fold increase). DO, dissolved oxygen;

NH_3, ammonia; TOC, total organic carbon; T6SS, Type VI secretion system; XD/T, xenobiotic degradation to translation ratio.

Fig 9: Conceptual framework of dry-season stress-induced microbiome restructuring. The cascade from environmental drivers (↓DO, ↑NH_3, ↑TOC) to metabolic retraction (↓86% amino acids, ↓69% energy, ↓74% translation), microbial enrichment (xenobiotic degraders and pathogens), virulence shifts (↑motility +14.2, ↑biofilm +2.2, ↑T6SS; ↓iron -5.7, ↓immune -3.4), ecological mechanisms, outcomes, and the XD/T stress index (18-fold increase).

4.8 Limitations and future directions

This study is limited by its reliance on DNA-level metagenomic potential, which may not directly correspond to expressed phenotypes. We examined only two time points and did not resolve taxonomic identities in detail. Future metatranscriptomic and isolation-based studies are needed to confirm that the functional shifts are realized at the protein level and to identify the specific bacterial lineages driving these changes. Additionally, while our analysis focused on planktonic communities, sediment and epilithic biofilm communities may harbor distinct functional profiles [64,31]. Nevertheless, the dramatic, coherent functional restructuring we document unveils a fundamental ecological principle: as dry-season stress intensifies, the river microbiome transitions from a growth-oriented, anabolic community to one configured for survival, competition, and chemical defense with the unintended consequence of elevated pathogenicity potential. These findings highlight an urgent need to incorporate functional metagenomic monitoring into water

quality assessment, especially in tropical river systems facing escalating anthropogenic and climatic pressures.

5. Conclusions

Our time-series metagenomic analysis of the Shitalakshya River uncovered a coordinated functional shift from primary metabolism to pollutant degradation and stress adaptation, accompanied by a profound remodelling of the virulence gene landscape. Motility, biofilm formation, and T6SS-mediated competition were strongly selected, while iron acquisition and immune evasion traits declined. These changes paralleled a severe deterioration in water quality, linking the microbiome functional signature to the magnitude of organic pollution. The results provide a systems-level understanding of how anthropogenic inputs re-engineer the river microbiome through strong ecological filtering, with direct implications for water quality monitoring and public health risk assessment. Future work integrating metatranscriptomics, isolate genomics, and spatial-temporal sampling will further resolve the active players and mechanisms underlying this dynamic response.

Acknowledgments

The authors thank Dhaka WASA for their valuable assistance with sample collection and logistical support during the fieldwork. This study was conducted as part of the Ph.D. research of M.E.H., who also gratefully acknowledges the University Grants Commission (UGC) of Bangladesh for providing a Ph.D. fellowship.

Funding

The authors received no specific funding for this work.

Conflict of interest

All authors declare that they have no conflicts of interest.

Author contributions

M.E.H.: Conceptualization, Investigation, Formal analysis, Writing—original draft.

M.S.R.: Methodology, Bioinformatics analysis, Writing—review & editing.

M.S.: Validation, Supervision, Writing—review & editing.

A.B.: Conceptualization, Supervision, Writing—review & editing.

Ethics statement

This article does not contain any studies with human participants or animals performed by any of the authors.

Data availability

The datasets generated during this study are available in the NCBI SRA repository under BioProject PRJNA1424261 (https://www.ncbi.nlm.nih.gov/bioproject/PRJNA1424261) (Accession: SAMN55380971 and SAMN55380975); S1 Dataset includes KEGG pathways, VFGs Abundance, and sequencing quality metrics (trimming, host filtering, and Kraken2-based microbial classification). All other relevant data are within the manuscript and its supporting information files.

ORCID

Muhammad Ehteshamul Haque; ID: https://orcid.org/0009-0001-0307-3243

Md. Shaminur Rahman; ID: https://orcid.org/0000-0002-3039-9337

Dr. Munawar Sultana; ID: https://orcid.org/0000-0002-8563-3661

Dr. Anowara Begum; ID: https://orcid.org/0000-0001-9915-3311

Correspondence and requests for materials should be addressed to **A. Begum.**

References

1. Abraham WR. Megacities as sources for pathogenic bacteria in rivers and their fate downstream. Int J Microbiol. 2011;2011:798292. doi: 10.1155/2011/798292
2. Mittal P, Prasoodanan PKV, Dhakan DB, Kumar S, Sharma VK. Metagenome of a polluted river reveals a reservoir of metabolic and antibiotic resistance genes. Environ Microbiome. 2019;14(1):5. doi: 10.1186/s40793-019-0345-3
3. Reddy B, Dubey SK. River Ganges water as reservoir of microbes with antibiotic and metal ion resistance genes: High throughput metagenomic approach. Environ Pollut. 2019;246:443-451. doi: 10.1016/j.envpol.2018.12.022
4. Serajuddin M, Chowdhury MAI, Haque ME. Assessing seasonal water quality variations using water quality index (WQI): A case study. Scholars J Eng Technol. 2019;7(8):245-251. doi: 10.36347/sjet.2019.v07i08.007
5. Bussi G, Shawal S, Hossain MA, Whitehead PG, Jin L. Multibranch modelling of flow and water quality in the Dhaka River system, Bangladesh: Impacts of future development plans and climate change. Water. 2023;15(17):3027. doi: 10.3390/w15173027
6. Haque ME, Kibria MG, Beauty SA, Sultana M, Akter S. Moving bed biofilm reactor (MBBR) technology for removal of emerging contaminants. In: Proceedings of the International Water Conference; 2025 Mar 19-20; Colombo, Sri Lanka.
7. Jaiswal D, Pandey J. Anthropogenically enhanced sediment oxygen demand creates mosaic of oxygen deficient zones in the Ganga River: Implications for river

health. Ecotoxicol Environ Saf. 2019;171:709-720. doi: 10.1016/j.ecoenv.2019.01.039

8. Parida PK, Behera BK, Dehury B, Rout AK, Sarkar DJ, Rai A, et al. Community structure and function of microbiomes in polluted stretches of river Yamuna in New Delhi, India, using shotgun metagenomics. Environ Sci Pollut Res. 2022;29(47):71311-71325. doi: 10.1007/s11356-022-20766-1
9. Morote-Sánchez B, Colomer J, Soler M, Gilabert J, Rodellas V, Garcia-Orellana J, et al. Aquatic deoxygenation associated with resuspension of anthropogenic organic matter. Water Res. 2025;278:123327. doi: 10.1016/j.watres.2025.123327
10. Behera BK, Sahu P, Rout AK, Parida PK, Sarkar DJ, Kaushik NK, et al. Exploring microbiome from sediments of River Ganga using a metagenomic approach. Aquat Ecosyst Health Manag. 2021;24(4):12-22. doi: 10.14321/aehm.024.04.04
11. Cheng H, Cheng L, Wang L, Zhu T, Cai W, Hua Z, et al. Changes of bacterial communities in response to prolonged hydrodynamic disturbances in the eutrophic water-sediment systems. Int J Environ Res Public Health. 2019;16(20):3868. doi: 10.3390/ijerph16203868
12. Behera BK, Chakraborty HJ, Patra B, Rout AK, Dehury B, Das BK, et al. Metagenomic analysis reveals bacterial and fungal diversity and their bioremediation potential from sediments of River Ganga and Yamuna in India. Front Microbiol. 2020;11:556136. doi: 10.3389/fmicb.2020.556136
13. Marathe NP, Pal C, Gaikwad SS, Jonsson V, Kristiansson E, Larsson DGJ. Untreated urban waste contaminates Indian river sediments with resistance genes

to last-resort antibiotics. Water Res. 2017;124:388-397. doi: 10.1016/j.watres.2017.07.060

14. Yadav R, Rajput V, Dharne M. Functional metagenomic landscape of polluted river reveals potential genes involved in degradation of xenobiotic pollutants. Environ Res. 2021;192:110332. doi: 10.1016/j.envres.2020.110332
15. Edirisinghe JN, Weisenhorn P, Conrad N, Xia F, Overbeek R, Stevens RL, et al. Modeling central metabolism and energy biosynthesis across microbial life. BMC Genomics. 2016;17:568. doi: 10.1186/s12864-016-2887-8
16. Brooks AN, Turkarslan S, Beer KD, Lo FY, Baliga NS. Adaptation of cells to new environments. Wiley Interdiscip Rev Syst Biol Med. 2011;3(5):544-561. doi: 10.1002/wsbm.136
17. Mitchell A, Romano GH, Groisman B, Yona A, Dekel E, Kupiec M, et al. Adaptive prediction of environmental changes by microorganisms. Nature. 2009;460(7252):220-224. doi: 10.1038/nature08112
18. Srivastava A, Verma D. Ganga River sediments of India predominate with aerobic and chemo-heterotrophic bacteria majorly engaged in the degradation of xenobiotic compounds. Environ Sci Pollut Res. 2023;30(3):752-772. doi: 10.1007/s11356-022-22198-3
19. Johnson J, Jain KR, Patel A, Parmar N, Joshi C, Madamwar D. Chronic industrial perturbation and seasonal change induces shift in the bacterial community from Gammaproteobacteria to Betaproteobacteria having catabolic potential for aromatic compounds at Amlakhadi canal. World J Microbiol Biotechnol. 2024;40(2):52. doi: 10.1007/s11274-023-03848-1

20. Rout AK, Dehury B, Parida PK, Sarkar DJ, Behera B, Das BK, et al. Taxonomic profiling and functional gene annotation of microbial communities in sediment of River Ganga at Kanpur, India: Insights from whole-genome metagenomics study. Environ Sci Pollut Res. 2022;29(54):82309-82323. doi: 10.1007/s11356-022-21644-6
21. Coulthurst SJ. The Type VI secretion system—A widespread and versatile cell targeting system. Res Microbiol. 2013;164(6):640-654. doi: 10.1016/j.resmic.2013.03.017
22. Ho BT, Dong TG, Mekalanos JJ. A view to a kill: The bacterial type VI secretion system. Cell Host Microbe. 2014;15(1):9-21. doi: 10.1016/j.chom.2013.11.008
23. Roges EM, Gonçalves VD, Cardoso MD, Festivo ML, Siciliano S, Berto LH, et al. Virulence-associated genes and antimicrobial resistance of Aeromonas hydrophila isolates from animal, food, and human sources in Brazil. Biomed Res Int. 2020;2020:1052607. doi: 10.1155/2020/1052607
24. Rout AK, Tripathy PS, Dixit S, Behera DU, Behera B, Das BK, et al. Unveiling the microbiome landscape: A metagenomic study of bacterial diversity, antibiotic resistance, and virulence factors in the sediments of the River Ganga, India. Antibiotics. 2023;12(12):1735. doi: 10.3390/antibiotics12121735
25. Shayan MNM, Tanaka Y, Shinji A, Nakayama T, Hirano R, Kuroda K, et al. Resuscitation, regrowth, and release of bacteria in biofilm in a river receiving chlorinated reclaimed water. Water Res X. 2026;31:100524. doi: 10.1016/j.wroa.2026.100524

26. Mao G, Liang J, Wang Q, Zhao C, Bai Y, Liu R, et al. Epilithic biofilm as a reservoir for functional virulence factors in wastewater-dominant rivers after WWTP upgrade. J Environ Sci (China). 2021;101:27-35. doi: 10.1016/j.jes.2020.05.014
27. Zou Y, Xiao Z, Wang L, Wang Y, Yin H, Li Y. Prevalence of antibiotic resistance genes and virulence factors in the sediment of WWTP effluent-dominated rivers. Sci Total Environ. 2023;897:165441. doi: 10.1016/j.scitotenv.2023.165441
28. Sahoo S, Sahoo RK, Gaur M, Behera DU, Sahu A, Das A, et al. Urban wastewater contributes to the emergence of carbapenem-resistant Klebsiella pneumoniae (CRKP) in an urban receiving river in eastern India. Lett Appl Microbiol. 2023;76(1):ovac005. doi: 10.1093/lambio/ovac005
29. Wang J, Wang Y, Lou H, Wang W. AlgU controls environmental stress adaptation, biofilm formation, motility, pyochelin synthesis and antagonism potential in Pseudomonas protegens SN15-2. Microbiol Res. 2023;272:127396. doi: 10.1016/j.micres.2023.127396
30. Parwin N, Dixit S, Das S, Sahoo RK, Subudhi E. Metagenomic analysis of microbiome spatial dynamics in urban river confluence affected by city wastewater. Genomics Inform. 2025;23:27. doi: 10.1186/s44342-025-00054-3
31. Parwin N, Dixit S, Subudhi E. From city waste to river risk: tracking AMR and pathogenic potential in urban water gradient of the Kathajodi river. Environ Sci Eur. 2026;38:64. doi: 10.1186/s12302-026-01347-2
32. Xie Y, Liu X, Wei H, Chen X, Gong N, Ahmad S, et al. Insight into impact of sewage discharge on microbial dynamics and pathogenicity in river ecosystem. Sci Rep. 2022;12(1):6894. doi: 10.1038/s41598-022-09579-x

807 33. Liu B, Zheng D, Jin Q, Chen L, Yang J. VFDB 2019: A comparative pathogenomic
808 platform with an interactive web interface. Nucleic Acids Res. 2019;47(D1):D687-
809 D692. doi: 10.1093/nar/gky1080
810 34. Rice EW, Baird RB, Eaton AD, Clesceri LS, editors. Standard methods for the
811 examination of water and wastewater. 22nd ed. Washington (DC): American Public
812 Health Association, American Water Works Association, Water Environment
813 Federation; 2012.
814 35. Jones A, Stanley D, Ferguson S, Schwessinger B, Borevitz J, Warthmann N. Cost-
815 conscious generation of multiplexed short-read DNA libraries for whole-genome
816 sequencing. PLoS ONE. 2023;18(1):e0280004. doi:
817 10.1371/journal.pone.0280004
818 36. Andrews S. FastQC: a quality control tool for high-throughput sequence data
819 [software]. Cambridge (UK): Babraham Institute; 2010. Available
820 from: https://www.bioinformatics.babraham.ac.uk/projects/fastqc/
821 37. Bolger AM, Lohse M, Usadel B. Trimmomatic: a flexible trimmer for Illumina
822 sequence data. Bioinformatics. 2014;30(15):2114-2120. doi:
823 10.1093/bioinformatics/btu170
824 38. Bushnell B. BBMap: a fast, accurate, splice-aware aligner [software].
825 SourceForge; 2014.
826 39. Wood DE, Lu J, Langmead B. Improved metagenomic analysis with Kraken 2.
827 Genome Biol. 2019;20(1):257. doi: 10.1186/s13059-019-1891-0

40. Lu J, Breitwieser FP, Thielen P, Salzberg SL. Bracken: estimating species abundance in metagenomics data. PeerJ Comput Sci. 2017;3:e104. doi: 10.7717/peerj-cs.104
41. Shen W, Ren H. TaxonKit: a practical and efficient NCBI taxonomy toolkit. J Genet Genomics. 2021;48(9):844-850. doi: 10.1016/j.jgg.2021.03.006
42. Bonin N, Doster E, Worley H, Pinnell LJ, Bravo JE, Ferm P, et al. MEGARes and AMR++, v3.0: an updated comprehensive database of antimicrobial resistance determinants. Nucleic Acids Res. 2023;51(D1):D744-D752. doi: 10.1093/nar/gkac1043
43. Chen L, Yang J, Yu J, Yao Z, Sun L, Shen Y, et al. VFDB: a reference database for bacterial virulence factors. Nucleic Acids Res. 2005;33(Database issue):D325-D328. doi: 10.1093/nar/gki008
44. Beghini F, McIver LJ, Blanco-Míguez A, Dubois L, Asnicar F, Maharjan S, et al. Integrating taxonomic, functional, and strain-level profiling of diverse microbial communities with bioBakery 3. eLife. 2021;10:e65088. doi: 10.7554/eLife.65088
45. Oksanen J, Blanchet FG, Kindt R, Legendre P, Minchin PR, O'Hara RB, et al. vegan: community ecology package (Version 2.0-10) [R package]. CRAN. 2013. Available from: https://CRAN.R-project.org/package=vegan
46. Gu Z, Gu L, Eils R, Schlesner M, Brors B. circlize: circular visualization in R. Bioinformatics. 2014;30(19):2811-2812. doi: 10.1093/bioinformatics/btu393
47. Rout AK, Tripathy PS, Dixit S, Behera DU, Behera B, Das BK, et al. Metagenomics analysis of sediments of river Ganga, India for bacterial diversity, functional

genomics, antibiotic resistant genes and virulence factors. Curr Res Biotechnol. 2024;7:100187. doi: 10.1016/j.crbiot.2024.100187

48. Rout AK, Rout SS, Panda A, Tripathy PS, Kumar N, Parida SN, et al. Potential applications and future prospects of metagenomics in aquatic ecosystems. Gene. 2025;967:149720. doi: 10.1016/j.gene.2025.149720

49. Behera BK, Patra B, Chakraborty HJ, Sahu P, Rout AK, Sarkar DJ, et al. Metagenome analysis from the sediment of river Ganga and Yamuna: In search of beneficial microbiome. PLoS ONE. 2020;15(10):e0239594. doi: 10.1371/journal.pone.0239594

50. Rout AK, Dixit S, Tripathy PS, Rout SS, Parida SN, Parida PK, et al. Metagenomic landscape of sediments of river Ganga reveals microbial diversity, potential plastic and xenobiotic degradation enzymes. J Hazard Mater. 2024;471:134377. doi: 10.1016/j.jhazmat.2024.134377

51. Potrykus K, Cashel M. (p)ppGpp: still magical? Annu Rev Microbiol. 2008;62:35-51. doi: 10.1146/annurev.micro.62.081307.162903

52. Battesti A, Majdalani N, Gottesman S. The RpoS-mediated general stress response in Escherichia coli. Annu Rev Microbiol. 2011;65:189-213. doi: 10.1146/annurev-micro-090110-102946

53. Behera BK, Patra B, Chakraborty HJ, Rout AK, Dixit S, Rai A, et al. Bacteriophages diversity in India's major river Ganga: A repository to regulate pathogenic bacteria in the aquatic environment. Environ Sci Pollut Res. 2023;30(12):34101-34114. doi: 10.1007/s11356-022-24637-7

54. Li Y, Jing H, Kao SJ, Zhang W, Liu H. Metabolic response of prokaryotic microbes to sporadic hypoxia in a eutrophic subtropical estuary. Mar Pollut Bull. 2020;154:111064. doi: 10.1016/j.marpolbul.2020.111064

55. Colin R, Ni B, Laganenka L, Sourjik V. Multiple functions of flagellar motility and chemotaxis in bacterial physiology. FEMS Microbiol Rev. 2021;45(6):fuab038. doi: 10.1093/femsre/fuab038

56. Yin W, Wang Y, Liu L, He J. Biofilms: the microbial "protective clothing" in extreme environments. Int J Mol Sci. 2019;20(14):3423. doi: 10.3390/ijms20143423

57. Serajuddin M, Chowdhury MAI, Haque MM, Haque ME. Using turbidity to determine total suspended solids in an urban stream: a case study. Int J Eng Trends Technol. 2019;67(9):83-88. doi: 10.14445/22315381/IJETT-V67I9P214

58. Sivadon P, Barnier C, Urios L, Grimaud R. Biofilm formation as a microbial strategy to assimilate particulate substrates. Environ Microbiol Rep. 2019;11(6):749-764. doi: 10.1111/1758-2229.12785

59. Zhang H, Chen G, Sun Z, Zhang X, Jiang Z, Zhang X. The microstructures of Tetradesmus obliquus biofilms formed under different nutrient supplies. Appl Sci. 2025;15(9):5104. doi: 10.3390/app15095104

60. Gallique M, Bouteiller M, Merieau A. The Type VI Secretion System: a dynamic system for bacterial communication? Front Microbiol. 2017;8:1454. doi: 10.3389/fmicb.2017.01454

61. Gonzalez Moreno PJ, Nishiguchi MK. The competitive edge: T6SS-mediated interference competition by Vibrionaceae across marine ecological niches. Microorganisms. 2025;13(6):1370. doi: 10.3390/microorganisms13061370

62. Galán JE, Lara-Tejero M, Marlovits TC, Wagner S. Bacterial type III secretion systems: Specialized nanomachines for protein delivery into target cells. Annu Rev Microbiol. 2014;68:415-438. doi: 10.1146/annurev-micro-092412-155725

63. Webb SA, Kahler CM. Bench-to-bedside review: Bacterial virulence and subversion of host defences. Crit Care. 2008;12(6):234. doi: 10.1186/cc7091

64. Lawrence JR, Chenier MR, Roy R, Beaumier D, Fortin N, Swerhone GD, et al. Microscale and molecular assessment of impacts of nickel, nutrients, and oxygen level on structure and function of river biofilm communities. Appl Environ Microbiol. 2004;70(7):4326-4339. doi: 10.1128/AEM.70.7.4326-4339.2004

65. Nakamura S, Minamino T. Flagella-driven motility of bacteria. Biomolecules. 2019;9(7):279. doi: 10.3390/biom9070279

Supporting information

S1 Dataset. Sequencing quality control metrics and KEGG pathway abundances. Includes trimming efficiency, host-read removal statistics, Kraken2-based microbial classification, and complete KEGG pathway relative abundances for both time points. (Provide filename: S1 Dataset.xlsx)

S1 Table. Physicochemical parameters at the Sarulia intake point during the early dry season (December 2024) and peak dry season (February 2025). (Provide filename: S1 Table.docx)

S2 Table. Key Xenobiotic-Degrading Bacteria Enriched in February 2025 (Provide filename: S2 Table.docx)

S3 Table. Disease-Associated Microorganisms Enriched from December 2024 to February 2025. (Provide filename: S3 Table.docx)

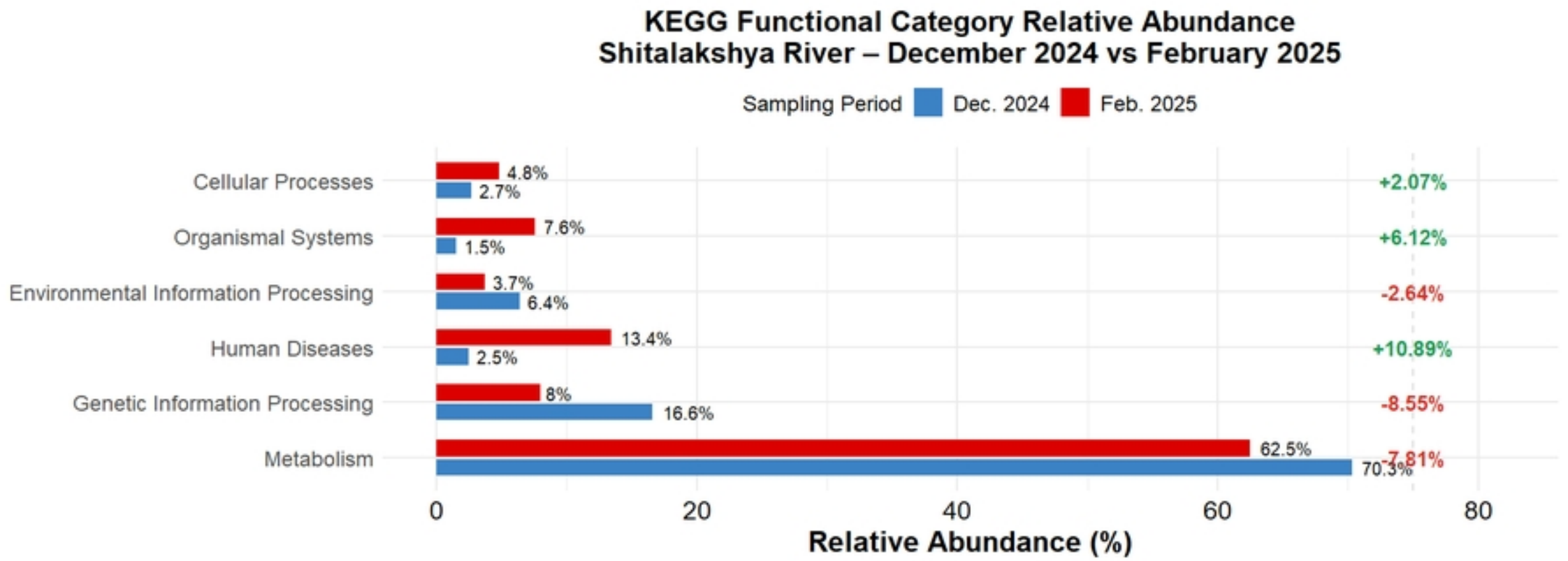
KEGG Functional Category Relative Abundance
Shitalakshya River – December 2024 vs February 2025
Sampling Period
Dec. 2024
Feb. 2025
Cellular Processes
4.8%
2.7%
+2.07%
Organismal Systems
7.6%
1.5%
+6.12%
Environmental Information Processing
3.7%
6.4%
-2.64%
Human Diseases
13.4%
2.5%
+10.89%
Genetic Information Processing
8%
16.6%
-8.55%
Metabolism
62.5%
70.3%
-7.81%
0
20
40
60
80
Relative Abundance (%)

Fig 1

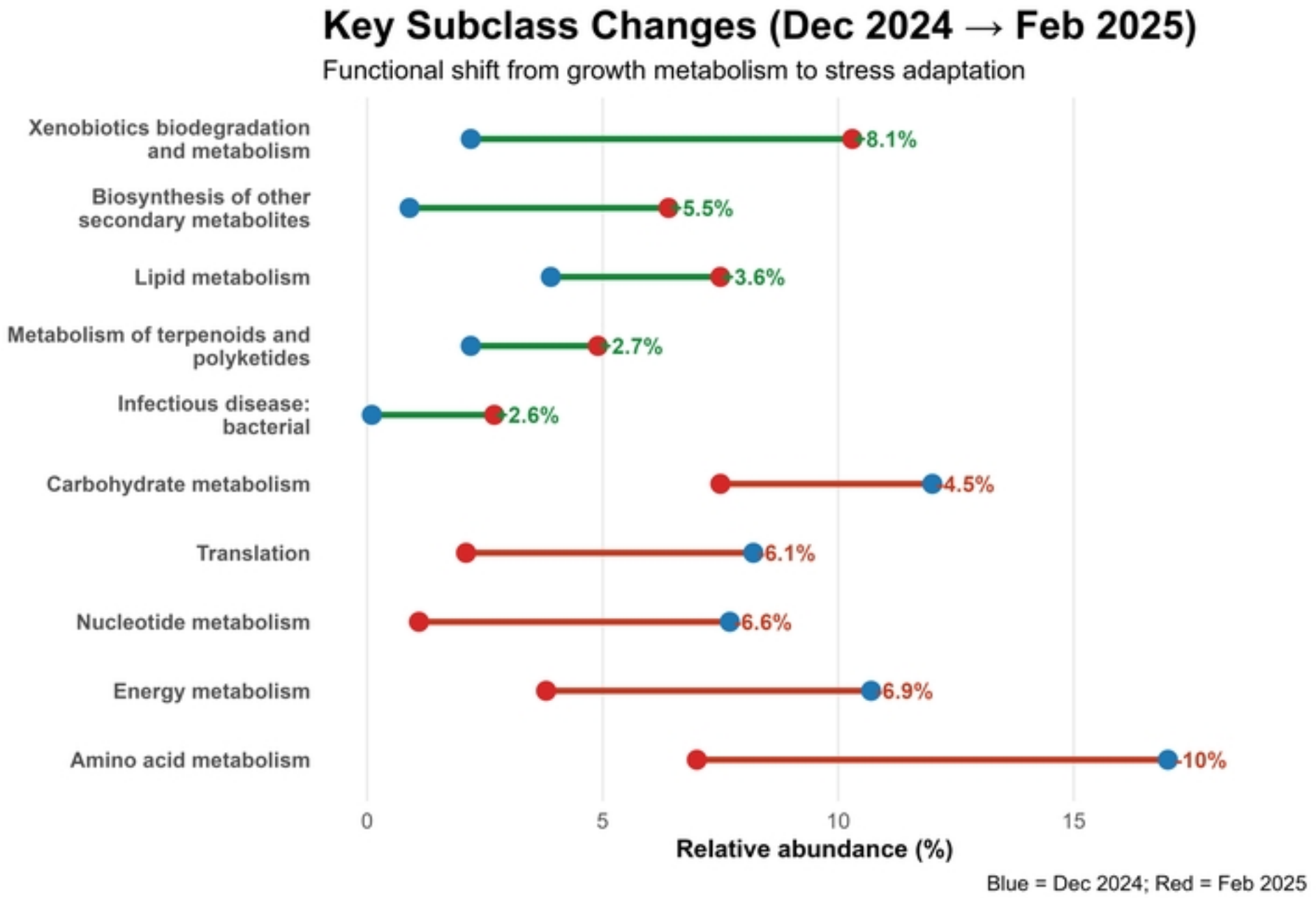
Key Subclass Changes (Dec 2024 → Feb 2025)
Functional shift from growth metabolism to stress adaptation
Xenobiotics biodegradation and metabolism
8.1%
Biosynthesis of other secondary metabolites
5.5%
Lipid metabolism
3.6%
Metabolism of terpenoids and polyketides
2.7%
Infectious disease: bacterial
2.6%
Carbohydrate metabolism
4.5%
Translation
6.1%
Nucleotide metabolism
6.6%
Energy metabolism
6.9%
Amino acid metabolism
10%
0
5
10
15
Relative abundance (%)
Blue = Dec 2024; Red = Feb 2025

Fig 2

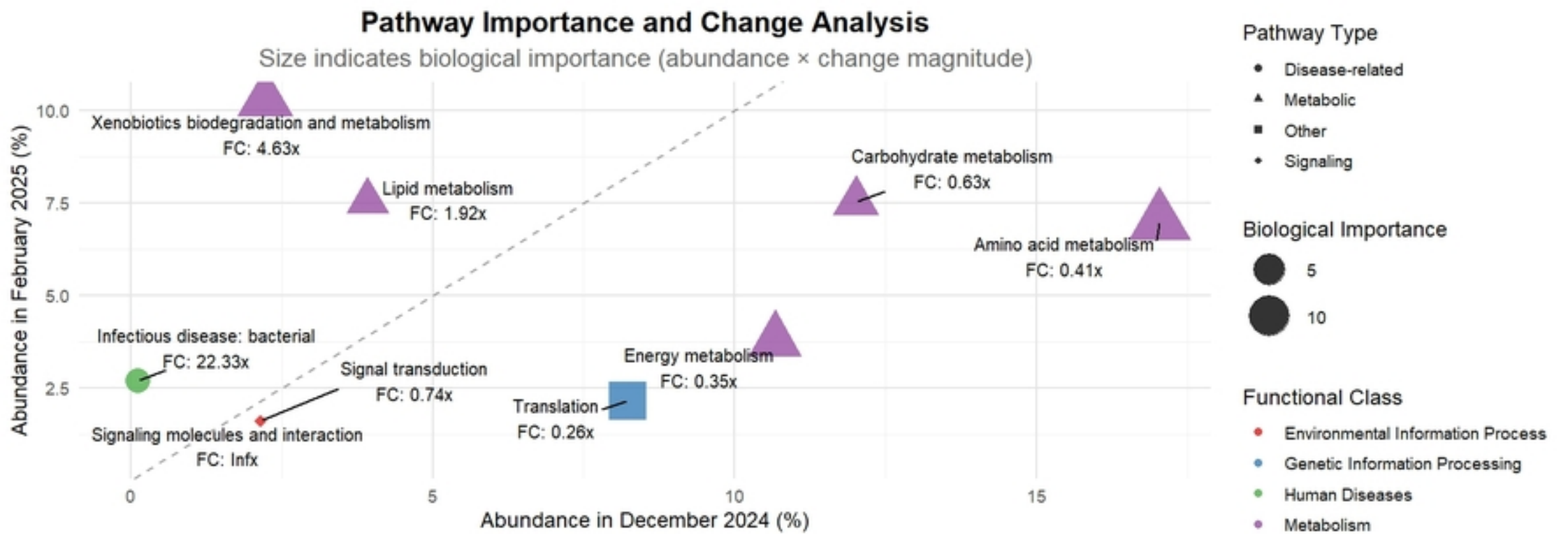
Pathway Importance and Change Analysis
Size indicates biological importance (abundance × change magnitude)
Abundance in February 2025 (%)
Abundance in December 2024 (%)
10.0
7.5
5.0
2.5
0
5
10
15
Xenobiotics biodegradation and metabolism
FC: 4.63x
Lipid metabolism
FC: 1.92x
Carbohydrate metabolism
FC: 0.63x
Amino acid metabolism
FC: 0.41x
Infectious disease: bacterial
FC: 22.33x
Signal transduction
FC: 0.74x
Energy metabolism
FC: 0.35x
Translation
FC: 0.26x
Signaling molecules and interaction
FC: Infx
Pathway Type
Disease-related
Metabolic
Other
Signaling
Biological Importance
5
10
Functional Class
Environmental Information Process
Genetic Information Processing
Human Diseases
Metabolism

Fig 3

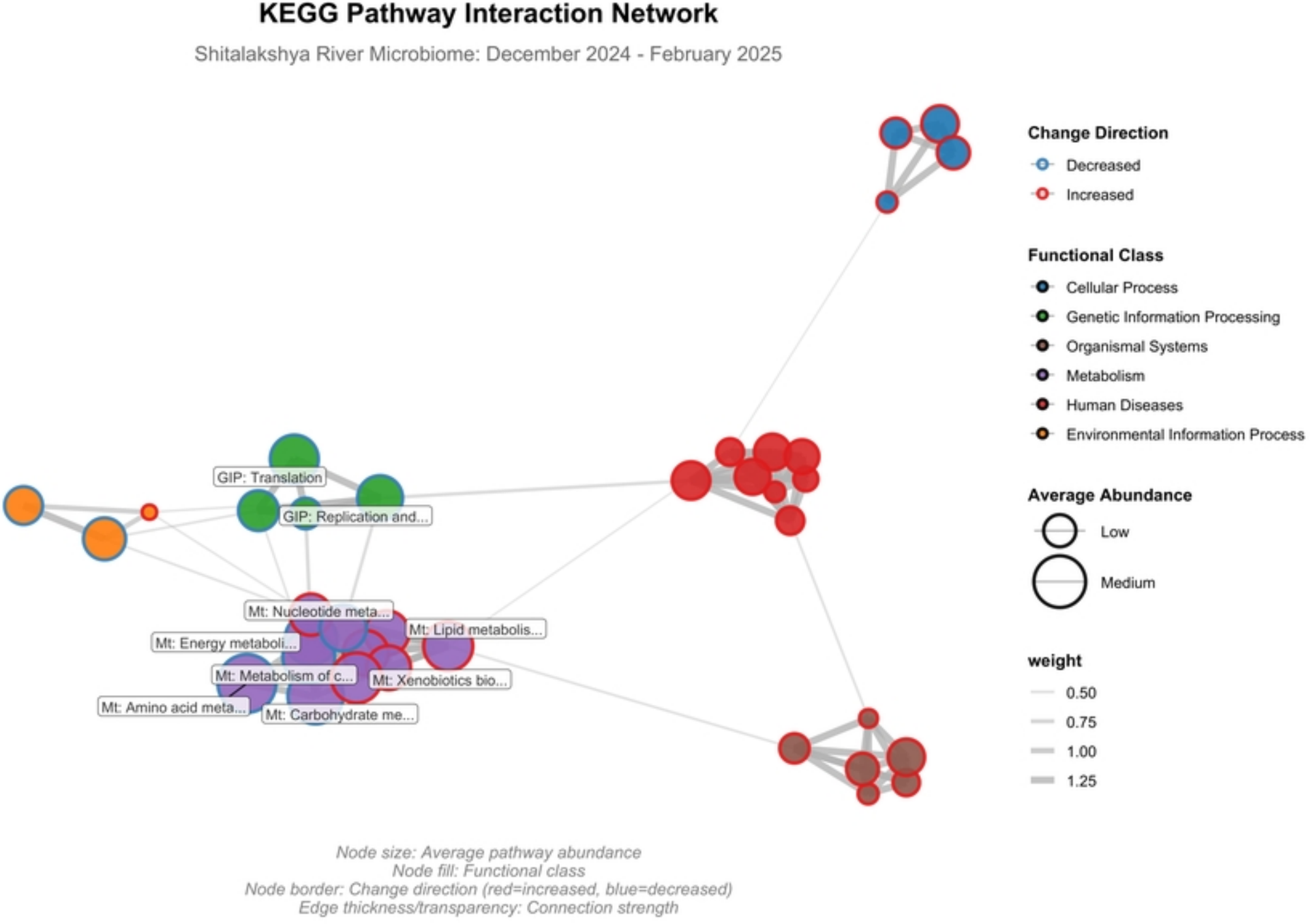
KEGG Pathway Interaction Network
Shitalakshya River Microbiome: December 2024 - February 2025
GIP: Translation
GIP: Replication and...
Mt: Nucleotide meta...
Mt: Lipid metabolis...
Mt: Energy metaboli...
Mt: Metabolism of c...
Mt: Xenobiotics bio...
Mt: Amino acid meta...
Mt: Carbohydrate me...
Change Direction
Decreased
Increased
Functional Class
Cellular Process
Genetic Information Processing
Organismal Systems
Metabolism
Human Diseases
Environmental Information Process
Average Abundance
Low
Medium
weight
0.50
0.75
1.00
1.25
Node size: Average pathway abundance
Node fill: Functional class
Node border: Change direction (red=increased, blue=decreased)
Edge thickness/transparency: Connection strength

Fig 4

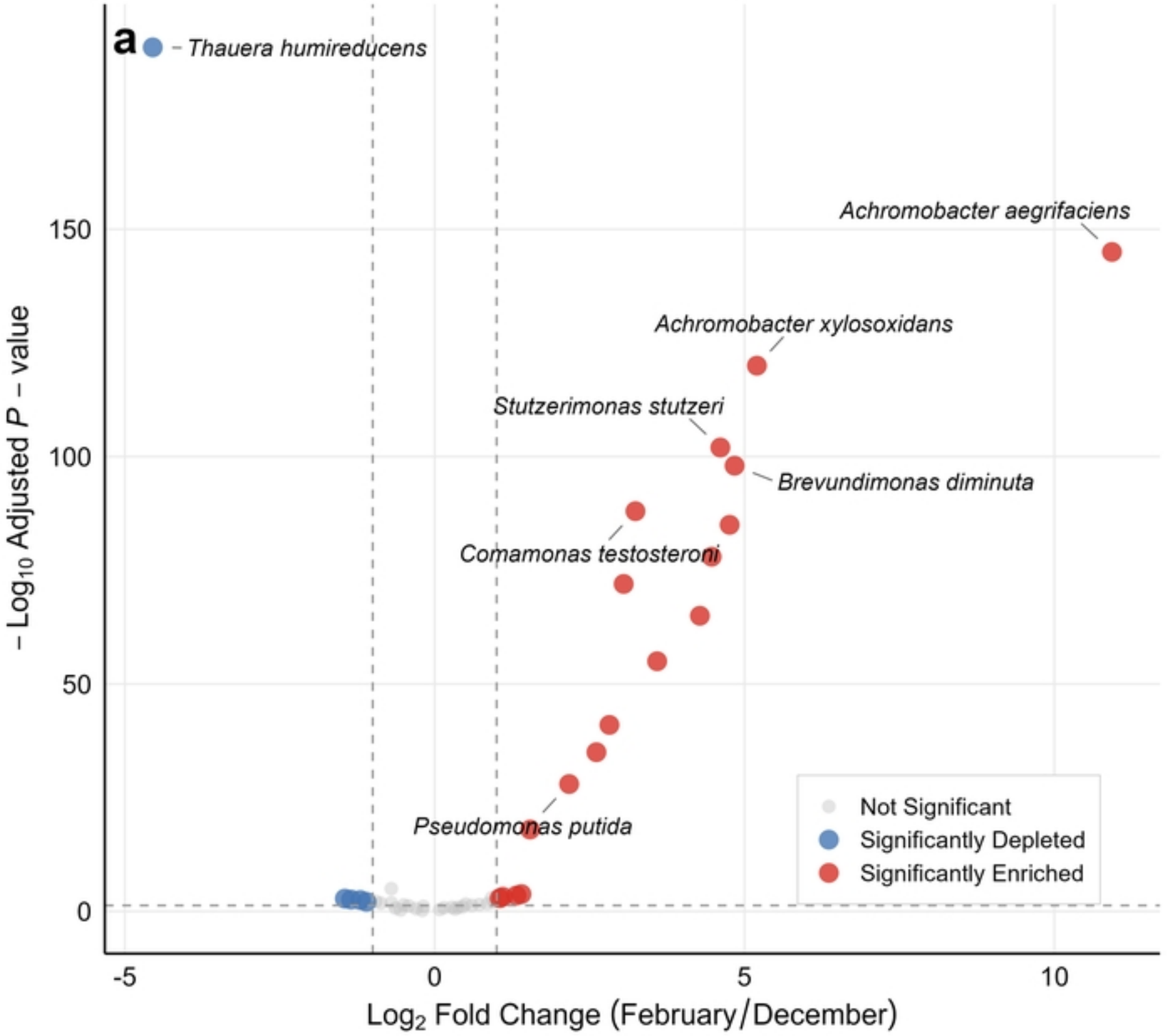
a
Thauera humireducens
Achromobacter aegrifaciens
Achromobacter xylosoxidans
Stutzerimonas stutzeri
Brevundimonas diminuta
Comamonas testosteroni
Pseudomonas putida
Not Significant
Significantly Depleted
Significantly Enriched
150
100
50
0
-5
0
5
10
– Log10 Adjusted P – value
Log2 Fold Change (February/December)

Fig 5a

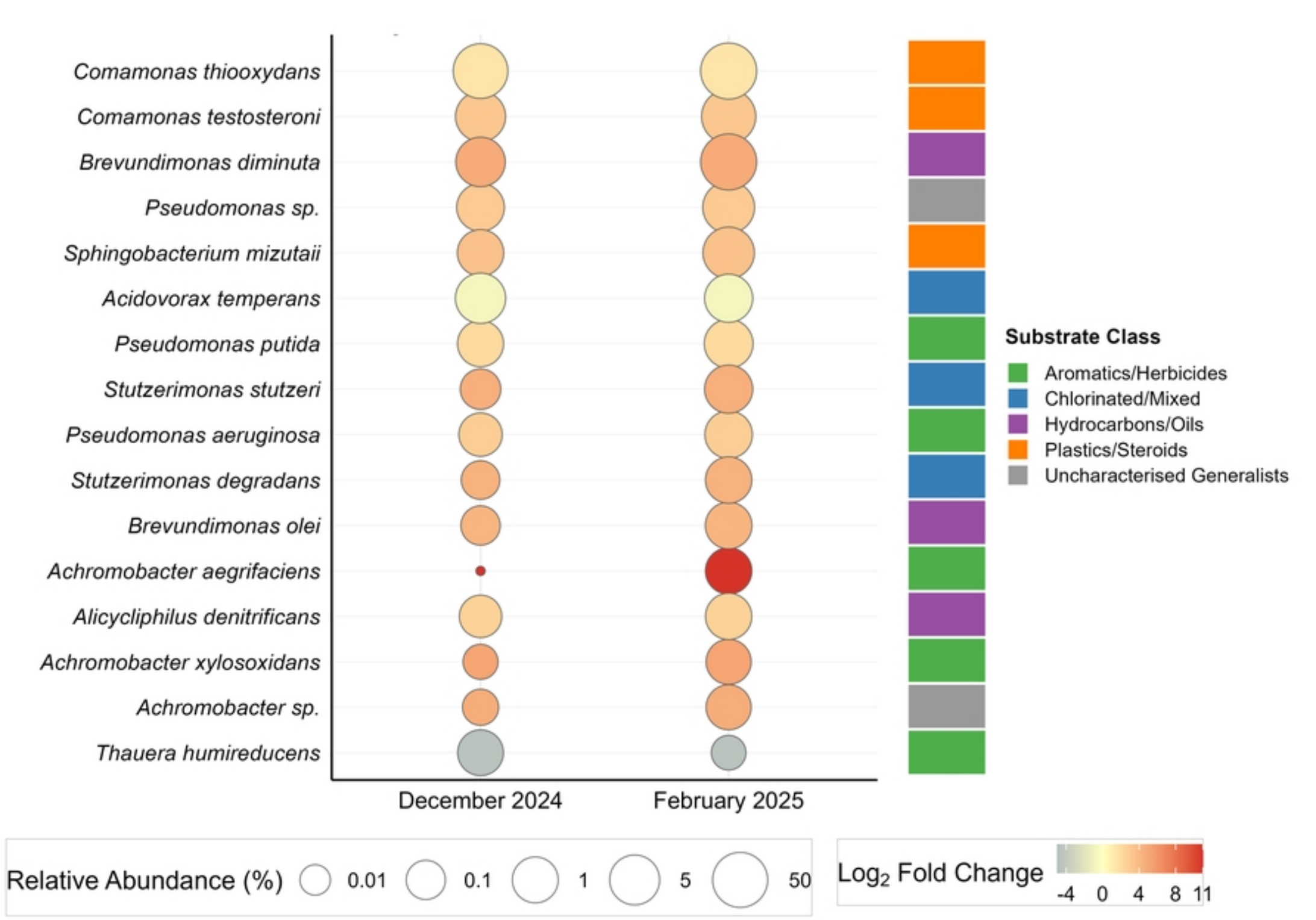
Comamonas thiooxydans
Comamonas testosteroni
Brevundimonas diminuta
Pseudomonas sp.
Sphingobacterium mizutaii
Acidovorax temperans
Pseudomonas putida
Stutzerimonas stutzeri
Pseudomonas aeruginosa
Stutzerimonas degradans
Brevundimonas olei
Achromobacter aegrifaciens
Alicycliphilus denitrificans
Achromobacter xylosoxidans
Achromobacter sp.
Thauera humireducens
December 2024
February 2025
Substrate Class
Aromatics/Herbicides
Chlorinated/Mixed
Hydrocarbons/Oils
Plastics/Steroids
Uncharacterised Generalists
Relative Abundance (%)
0.01
0.1
1
5
50
Log2 Fold Change
-4
0
4
8
11

Fig 5b

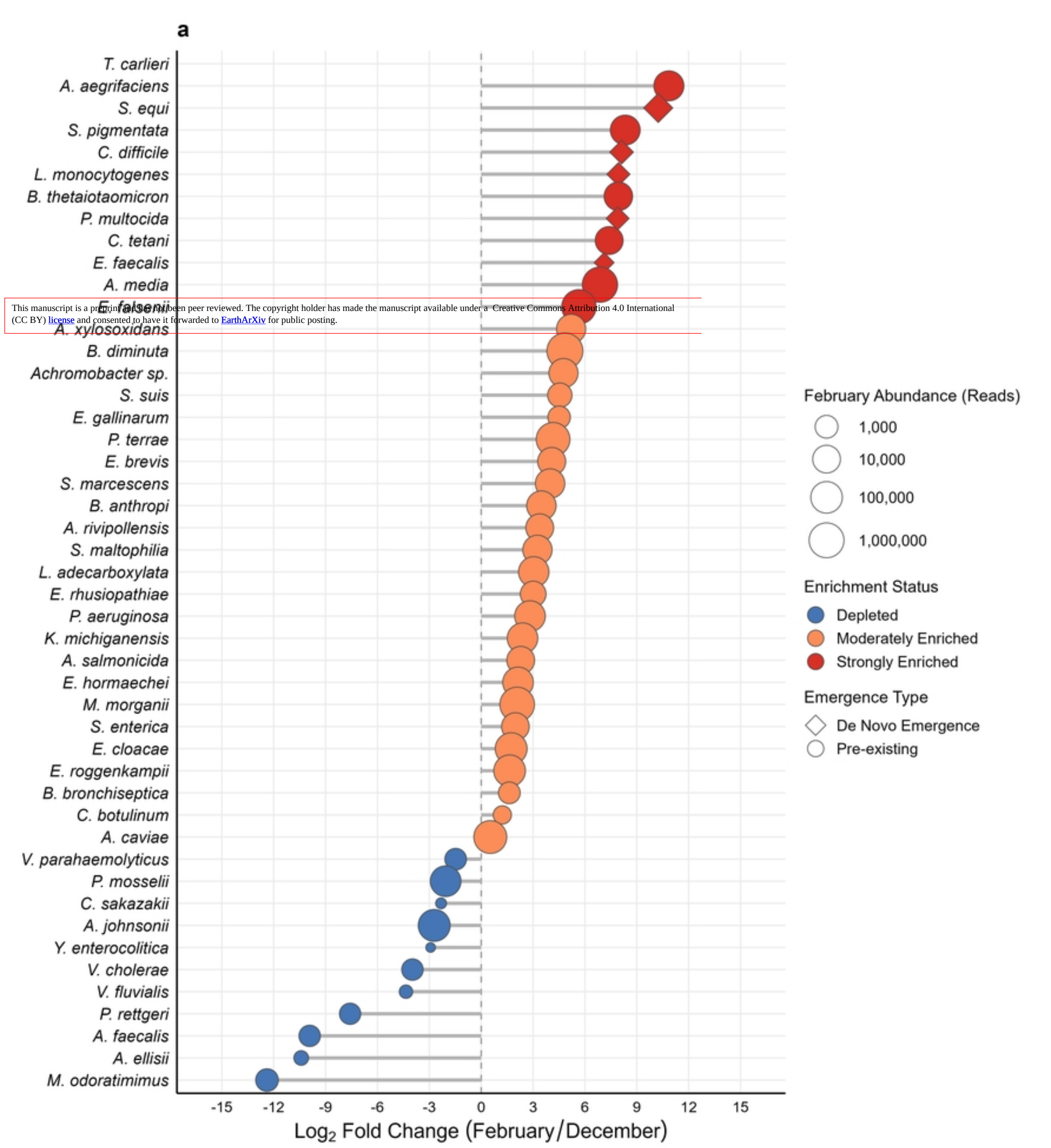

Fig 6

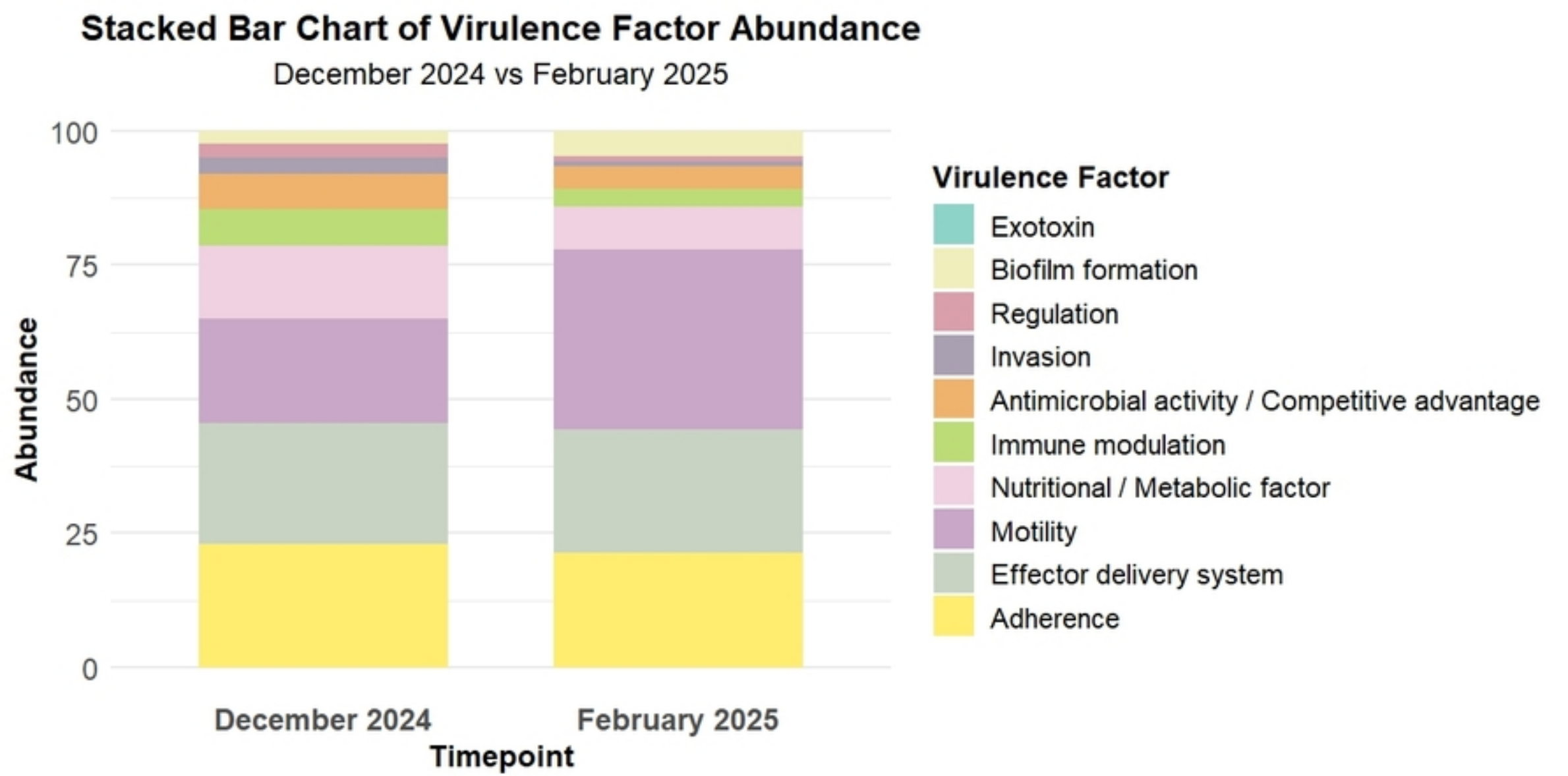
Stacked Bar Chart of Virulence Factor Abundance
December 2024 vs February 2025
100
75
50
25
0
Abundance
December 2024
February 2025
Timepoint
Virulence Factor
Exotoxin
Biofilm formation
Regulation
Invasion
Antimicrobial activity / Competitive advantage
Immune modulation
Nutritional / Metabolic factor
Motility
Effector delivery system
Adherence

Fig 7

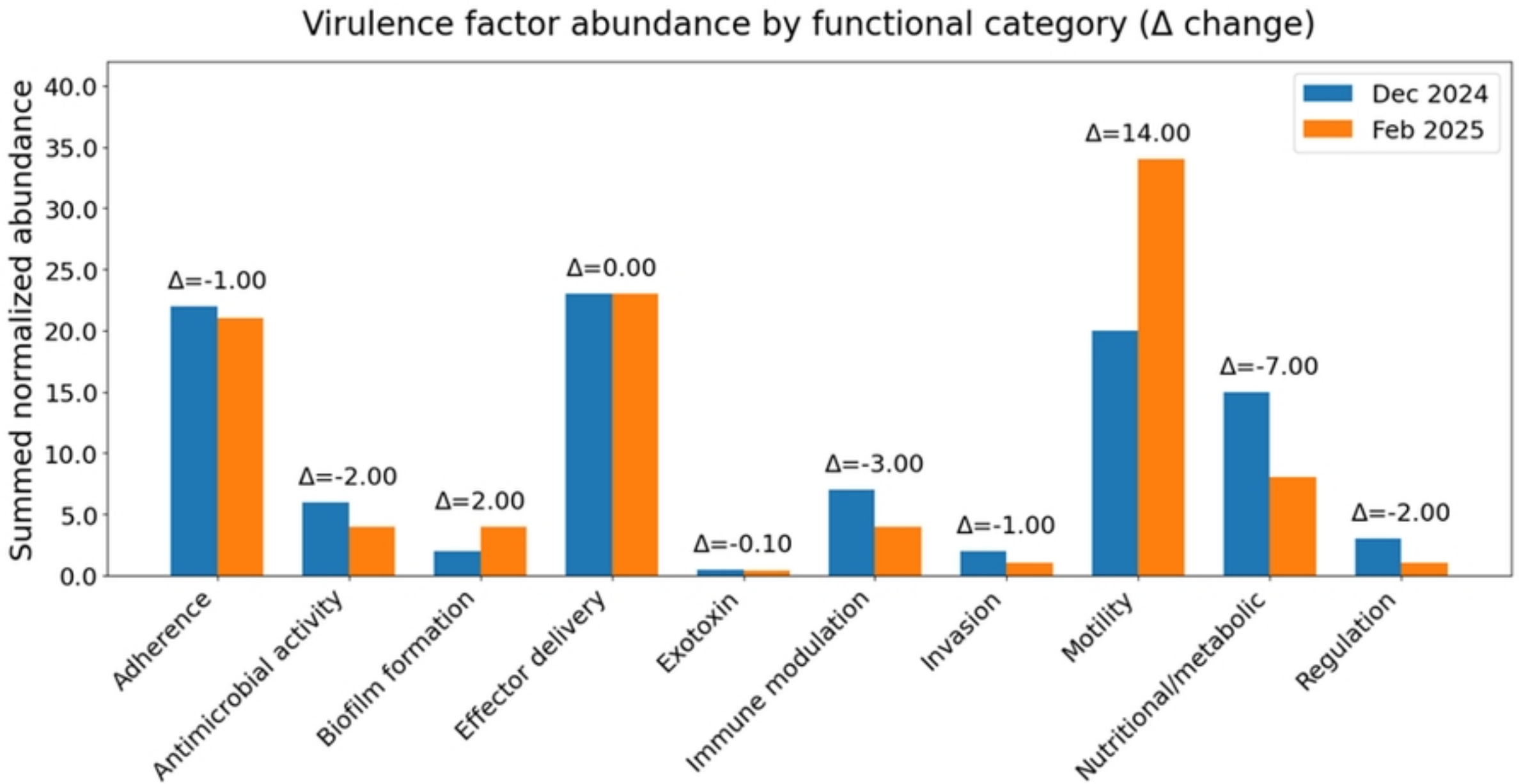
Virulence factor abundance by functional category (Δ change)
Summed normalized abundance
40.0
35.0
30.0
25.0
20.0
15.0
10.0
5.0
0.0
Dec 2024
Feb 2025
Δ=-1.00
Δ=-2.00
Δ=2.00
Δ=0.00
Δ=-0.10
Δ=-3.00
Δ=-1.00
Δ=14.00
Δ=-7.00
Δ=-2.00
Adherence
Antimicrobial activity
Biofilm formation
Effector delivery
Exotoxin
Immune modulation
Invasion
Motility
Nutritional/metabolic
Regulation

Fig 8

Fig 9